

*Work supported in part by the U. S. Atomic Energy Commission under Contract No. AT(11-1)1569.

†Present Address: Department of Physics and Astronomy, University of Massachusetts, Amherst, Mass. 01002.

¹L. H. Nosanow, *Phys. Rev.* **146**, 120 (1966), referred to as I.

²J. H. Hetherington, W. J. Mullin, and L. H. Nosanow *Phys. Rev.* **154**, 175 (1967), referred to as II.

³R. C. Pandorf and D. O. Edwards, *Phys. Rev.* **169**, 222 (1968).

⁴L. H. Nosanow and N. R. Werthamer, *Phys. Rev. Letters* **15**, 618 (1965); F. W. de Wette, L. H. Nosanow, and N. R. Werthamer, *Phys. Rev.* **162**, 824 (1967).

⁵T. R. Koehler, *Phys. Rev. Letters* **18**, 654 (1967); *Phys. Rev.* **165**, 942 (1968).

⁶H. Horner, *Z. Physik* **205**, 72 (1967).

⁷L. H. Nosanow and C. M. Varma, *Phys. Rev. Letters* **20**, 912 (1968).

⁸W. J. Mullin, *Phys. Rev. Letters* **20**, 254 (1968).

⁹L. H. Nosanow, in *Proceedings of the Eleventh International Conference on Low-Temperature Physics* edited by J. F. Allen, D. M. Finlayson, D. M. McCall

(University of St. Andrews Printing Department, St. Andrews, Scotland, 1969), Vol. I, p. 329.

¹⁰K. A. Brueckner and J. Froberg, *Progr. Theoret. Phys. (Kyoto), Suppl.*, 383 (1965).

¹¹J. Froberg, Ph.D. thesis, University of California, San Diego, 1967 (unpublished).

¹²K. A. Brueckner and R. Thieberger, *Phys. Rev.* **178**, 362 (1969).

¹³M. G. Richards, J. Hatton, and R. P. Giffard, *Phys. Rev.* **139**, A91 (1965).

¹⁴R. G. Richardson, E. Hunt, and H. Meyer, *Phys. Rev.* **138**, A1326 (1965).

¹⁵M. F. Panczyk, R. A. Scribner, G. C. Straty, and E. D. Adams, *Phys. Rev. Letters* **19**, 1102 (1967).

¹⁶E. D. Adams and M. F. Panczyk (unpublished).

¹⁷W. E. Massey and C.-W. Woo, *Phys. Rev.* **169**, 241 (1968); C.-W. Woo and W. E. Massey, *ibid.* (to be published).

¹⁸J. P. Hansen and D. Levesque, *Phys. Rev.* **165**, 293 (1968).

¹⁹G. Meisner, *Phys. Rev. Letters* **21**, 435 (1968).

²⁰R. A. Guyer (unpublished).

²¹H. Horner (private communication).

Amplitude Instability and Ergodic Behavior for Conservative Nonlinear Oscillator Systems*

Grayson H. Walker and Joseph Ford

School of Physics, Georgia Institute of Technology, Atlanta, Georgia 30332

(Received 27 March 1969)

Several earlier computer studies of nonlinear oscillator systems have revealed an amplitude instability marking a sharp transition from conditionally periodic to ergodic-type motion, and several authors have explained the observed instabilities in terms of a mathematical theorem due to Kolmogorov, Arnol'd, and Moser. In view of the significance of these results to several diverse fields, especially to statistical mechanics, this paper attempts to provide an elementary introduction to Kolmogorov-Arnol'd-Moser amplitude instability and to provide a verifiable scheme for predicting the onset of this instability. This goal is achieved by demonstrating that amplitude instability can occur even in simple oscillator systems which admit to a clear and detailed analysis. The analysis presented here is related to several earlier studies. Special attention is given to the relevance of amplitude instability for statistical mechanics.

I. INTRODUCTION

In attempting to determine the behavior of nonlinear oscillator systems governed by Hamiltonians of the form

$$H = H_0 + V, \quad (1)$$

where H_0 represents an integrable system of oscillators and where V represents a weak nonlinear

and nonintegrable perturbation, most investigators have proceeded along one of two divergent paths. One approach assumes that the weak perturbation V changes the unperturbed motion only to the extent of slightly shifting the frequencies of the motion and introducing small nonlinear harmonics. This approach is used most frequently when the number of oscillators is relatively small, and it is exemplified in certain perturbation expansions due to Poincare,¹ Birkhoff,² and Kryloff and

Bogoliubov.³ The second approach assumes that V , even though weak, has a profound and pathological effect on the unperturbed motion, converting it into ergodic⁴ motion. This latter approach uses the methods of statistical mechanics (presumed valid when the number of oscillators is large) and is exemplified in the work of Fermi⁵ and Peierls.⁶

A brief paper by Kolmogorov⁷ enunciated a theorem which can perhaps provide a cornerstone for linking the two aforementioned divergent views on the effects of the weak perturbation V in Eq. (1). Kolmogorov did not present a detailed proof of his theorem; the missing proof, which is quite long and mathematically sophisticated, was supplied almost a decade later by Arnol'd⁸ and independently by Moser.⁹ As a consequence perhaps, the physical scientist has largely remained unaware of Kolmogorov's theorem and its implications. For details of the theory with applications, the reader is referred to the review article by Arnol'd.¹⁰ However, in order to make this paper self-contained, we briefly present here those details of the theory relevant to this paper; in particular we may restrict our attention to systems with two degrees of freedom without significant loss of generality.

Introducing action-angle type variables (J_i, φ_i) for a two-oscillator system, Hamiltonian (1) may be written

$$H = H_0(J_1, J_2) + V(J_1, J_2, \varphi_1, \varphi_2). \quad (2)$$

If we set $V \equiv 0$, then Hamiltonian (2) generates motion for which the J 's are constant and $\varphi_i = \omega_i(J_1, J_2)t + \varphi_{i0}$, where the unperturbed frequencies ω_i are given by $\omega_i = \partial H_0 / \partial J_i$. Following Kolmogorov, we view the unperturbed system motion in phase space as lying on two-dimensional tori where (φ_1, φ_2) are the angle coordinates on the tori and (J_1, J_2) are the "radii" of the tori. By assuming that V is sufficiently small and by assuming that the Jacobian of the frequencies $\partial(\omega_1, \omega_2) / \partial(J_1, J_2) \neq 0$, Kolmogorov-Arnol'd-Moser (hereafter referred to as KAM) are able to show that most of the unperturbed tori bearing conditionally periodic motion with incommensurate frequencies continue to exist, being only slightly distorted by the perturbation. On the other hand, the tori bearing periodic motion, or very nearly periodic motion, with commensurate frequencies, or with incommensurate frequencies whose ratio is approximated extremely well by (r/s) where r and s are relatively small integers, are grossly deformed by the perturbation and no longer remain close to the unperturbed tori. Since the unperturbed tori with commensurate frequencies which are destroyed by the perturbation are everywhere dense, it is remarkable indeed that KAM are able to show that the majority - in the sense of measure theory - of initial conditions for Hamiltonian (2) lie

on the preserved tori bearing conditionally periodic motion when V is sufficiently small.

Thus for small V , KAM theory proves that for most initial conditions Hamiltonian (2) generates nonergodic motion thus justifying the view that the perturbation V largely serves only to slightly shift the frequencies and introduce small nonlinear harmonics into the motion.¹¹ Nonetheless, the relatively small set of initial conditions leading to motion not on preserved tori is, from a physical point of view, pathologically interspersed between the preserved tori. Moreover, Arnol'd¹⁰ conjectures that the system phase-space trajectory in regions of the destroyed tori is quite complicated indeed, perhaps ergodically filling the destroyed region. Thus, if Hamiltonian (2) is ever to provide generally ergodic motion best described in terms of statistical mechanics, the source of such behavior must lie in the reasons for the very existence of this relatively small set of destroyed tori. Hence we now investigate the properties of V which lead to the destruction of tori.

To this end, we expand the V of Hamiltonian (2) in a Fourier series and write

$$H = H_0(J_1, J_2) + \sum_{mn} f_{mn}(J_1, J_2) \times \cos(m\varphi_1 + n\varphi_2) + \dots, \quad (3)$$

where we have explicitly written only one term in the series. The KAM formalism seeks to eliminate the angle-dependent terms using a convergent sequence of canonical transformations, each of which is close to the identity transformation, thus obtaining a Hamiltonian which is a function of the transformed action variables alone and which is close to the original Hamiltonian. If this can be accomplished in some general sense, then one immediately finds that the perturbed motion, for the most part, lies on tori close to the unperturbed tori. As illustration, let us seek to eliminate the explicit angle-dependent term in Hamiltonian (3) by introducing the canonical transformation generated¹² by

$$F = \mathcal{J}_1 \varphi_1 + \mathcal{J}_2 \varphi_2 + B_{mn}(\mathcal{J}_1, \mathcal{J}_2) \sin(m\varphi_1 + n\varphi_2), \quad (4)$$

where $(\mathcal{J}_i, \theta_i)$ are the transformed action-angle variables and $B_{mn}(\mathcal{J}_1, \mathcal{J}_2)$ is to be determined. We note that if $B_{mn} = 0$, we have the identity transformation $J_i = \mathcal{J}_i$ and $\varphi_i = \theta_i$.

Introducing the canonical transformation generated by Eq. (4) into Hamiltonian (3), we obtain

$$H = H_0(\mathcal{J}_1, \mathcal{J}_2) + \{[m\omega_1(\mathcal{J}_1, \mathcal{J}_2) + n\omega_2(\mathcal{J}_1, \mathcal{J}_2)]$$

$$\times B_{mn}(\mathcal{J}_1, \mathcal{J}_2) + f_{mn}(\mathcal{J}_1, \mathcal{J}_2)\} \\ \cos(m\theta_1 + n\theta_2) + \dots, \quad (5)$$

where $\omega_i(\mathcal{J}_1, \mathcal{J}_2) = \partial H_0(\mathcal{J}_1, \mathcal{J}_2)/\partial \mathcal{J}_i$ and where we have explicitly retained only the lowest-order terms. We may now eliminate the given angle-dependent term, provided we set

$$B_{mn}(\mathcal{J}_1, \mathcal{J}_2) = - \frac{f_{mn}(\mathcal{J}_1, \mathcal{J}_2)}{m\omega_1(\mathcal{J}_1, \mathcal{J}_2) + n\omega_2(\mathcal{J}_1, \mathcal{J}_2)}, \quad (6)$$

and provided that the denominator in Eq. (6) is not very small (or zero) relative to f_{mn} . If the denominator in Eq. (6) is very small, then the coefficient B_{mn} is large, the transformation generated by Eq. (4) is not close to the identity transformation, and the transformed coordinate motion is not close to the unperturbed motion. As a consequence, if there exists a band of frequencies ω_i for Hamiltonian (3) satisfying

$$|m\omega_1(\mathcal{J}_1, \mathcal{J}_2) + n\omega_2(\mathcal{J}_1, \mathcal{J}_2)| \ll |f_{mn}(\mathcal{J}_1, \mathcal{J}_2)|, \quad (7)$$

then the angle-dependent term $\cos(m\varphi_1 + n\varphi_2)$ grossly distorts an associated zone of unperturbed tori bearing the frequencies satisfying the inequality (7).

Moreover, when a zone of unperturbed tori is grossly distorted by a specified angle-dependent term $\cos(m\varphi_1 + n\varphi_2)$, one must in general anticipate that there will be a host of angle-dependent terms $\cos(m'\varphi_1 + n'\varphi_2)$ in Hamiltonian (3) whose (m'/n') ratios are sufficiently close to the specified ratio (m/n) that the analog of the inequality (7) is satisfied for them also. Hence the zone of unperturbed tori distorted by $\cos(m\varphi_1 + n\varphi_2)$ will simultaneously be affected by a large number of other angle-dependent terms. Physically speaking, the inequality (7) is a resonance relationship which, if satisfied, asserts that $\cos(m\varphi_1 + n\varphi_2)$ resonantly couples the unperturbed oscillators when their frequencies lie in the designated band. If a number of angle-dependent resonant terms couple the oscillators in this band, then one has the situation envisioned in the quantum-mechanical Golden Rule¹³ in which an initial state is resonantly coupled to a density of final states leading to statistically irreversible behavior. In analogy, one would anticipate that the motion generated by Hamiltonian (3) in the overlapping resonant zones of destroyed tori is highly complicated, perhaps even ergodic.

When V is very small and hence all f_{mn} are small, the inequality (7) shows that the resonance zones are very narrow. Moreover, KAM show that the totality of all resonant destroyed zones is small¹⁴ relative to the measure of the allowed phase

space. However, as V and the f_{mn} increase, or equivalently as the total energy increases, one anticipates from the inequality (7) that the measure of the overlapping resonant zones may increase until most of phase space is filled with highly complicated trajectories moving under the influence of many resonances. In short, KAM theory indicates, but certainly does not prove, the existence of an amplitude instability for conservative nonlinear oscillator systems which permits a transition from motion which is predominantly conditionally periodic to motion which is predominantly ergodic. Since this transition lies outside the scope of KAM theory, we now review some of the computer generated evidence which supports the existence of an amplitude instability.

One of the first computer demonstrations of an amplitude instability was made in an investigation of unimolecular dissociation by Thiele and Wilson¹⁵ and by Bunker.¹⁶ These investigators noted that for small amplitude motion the harmonic modes of triatomic molecules exhibited very little energy exchange. As the energy of the molecule was increased, an amplitude instability occurred which allowed free and rapid interchange of energy between the harmonic modes. Consequently, as the energy was further increased to slightly above that needed to dissociate one atom from the molecule, almost all initial configurations led to dissociation. Thiele and Wilson¹⁵ then used these results to argue that nonlinearity must be given a central role in developing a statistical theory of unimolecular dissociation. These molecular systems were not analyzed in terms of the KAM theory; however, using the techniques discussed in the following paragraphs, the present authors have shown that the observed amplitude instability of Wilson's oscillator model occurs concurrently with a large-scale disappearance of preserved tori.

The second major computer demonstration of amplitude instability occurred in an astronomical study. Henon and Heiles¹⁷ studied the bounded motion of the system

$$H = \frac{1}{2}(p_1^2 + p_2^2 + q_1^2 + q_2^2) + q_1^2 q_2 - \frac{1}{3} q_2^3 \quad (8)$$

in order to determine whether or not a well-behaved constant of the motion exists for Hamiltonian (8) in addition to H itself. This study was motivated by empirical and theoretical evidence¹⁸ that a star moving in a cylindrically symmetric potential appeared to have a well-behaved constant of the motion in addition to the total energy and the z component of angular momentum. Since we intend to rely heavily in the main body of this paper on the techniques used by Henon and Heiles, we now outline their approach. The reader who finds the following discussion unclear is urged to read the extremely clear Henon and Heiles paper.

For fixed energy below the dissociation energy, all the phase-space trajectories generated by Hamiltonian (8) must lie on a bounded, three-dimensional energy surface. If an additional well-behaved constant of the motion $I(q_1, p_1, q_2, p_2)$ exists, then all system trajectories are further constrained to lie on bounded two-dimensional surfaces; if no well-behaved constant I exists, then the system trajectories will move randomly over some or all of the energy surface. If we now imagine a two-dimensional plane cutting through this three-dimensional energy surface, then the existence of a well-behaved constant I ensures that each system trajectory will intersect this plane along a curve, called a level curve; if a well-behaved I does not exist, the intersections of each trajectory will form a set of randomly scattered points. As a test then for the existence of a well-behaved constant I , Henon and Heiles integrated the equations of motion for Hamiltonian (8) and graphically plotted the intersection points of the system trajectory with the (q_2, p_2) plane determined¹⁹ by the conditions $q_1 = 0$ and $\dot{p}_1 \geq 0$. Using the Henon-Heiles method, we have integrated Hamiltonian (8) on a UNIVAC 1108 computer to obtain the level curves shown in Figs. 1-5.

Henon and Heiles analyzed these figures only in regard to constants of the motion. However, when the constants of the motion H and I restrict the system motion to lie on a two-dimensional surface in (q_1, p_1, q_2, p_2) space, one may use canonical transformation theory²⁰ to show that this two-dimensional surface is topologically equivalent to a KAM torus. A level curve in the (q_2, p_2) plane is thus topologically equivalent to a cross section of the torus. Figures 1-5 may then be regarded as profiles of KAM tori.

Figure 1, for energy $E = \frac{1}{12}$, shows that, to computer accuracy,²¹ all trajectories lie on tori. However, the inequality (7) makes it clear that there are zones of instability which could be observed with sufficient computer accuracy. Nonetheless, Fig. 1 demonstrates that $E = \frac{1}{12}$ is deep within the region of KAM stability. Figures 2 and 3 illustrate the characteristic behavior of the tori at the onset of macroscopic instability when the microscopic KAM zones of instability become large enough to be seen by the computer. Figure 2, at about $E = 0.106$, shows the appearance of a new type of torus which consists of a chain of eight islands surrounding the central invariant point on the upper p_2 axis. Figure 3 shows two zones on instability which appear simultaneously with the island chains; both instabilities characteristically first appear as a replacement for the self-intersecting curve of Fig. 1, called a separatrix. Jefferys²² explains this latter fact in terms of the KAM theory and the examples studied later in this paper support his explanation. Figure 4, at $E = \frac{1}{8}$, depicts the intermediate situation in which preserved tori still cover about 70% of the available area while intersections of the single orbit shown rather uniformly cover the re-

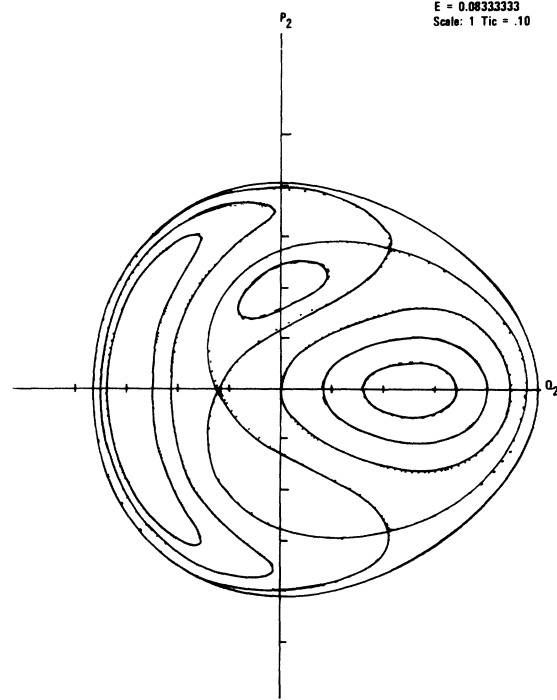


FIG. 1. Level curves for the Henon-Heiles system in the (q_2, p_2) plane. The microscopic zones of KAM instability lie below the computer integration accuracy. Here and in all level curve diagrams whenever a trajectory yields intersection points obviously lying on a smooth curve, the indicated curve has been drawn in freehand. The only exception occurs in Fig. 2 where the full level curves for the two chains of eight islands have not been freehanded in.

maining 30%. Figure 5, at the dissociation energy $E = \frac{1}{6}$, demonstrates that almost all the system motion is now statistical in character.

The final example of KAM instability is provided by the Hamiltonian system

$$H = \frac{1}{2} \sum_k (p_k^2 + \omega_k^2 q_k^2) + \alpha \sum_{i,j,k} A_{ijk} q_i q_j q_k + \lambda \sum_{h,i,j,k} B_{hijk} q_h q_i q_j q_k \quad (9)$$

originally proposed by Fermi, Pasta, and Ulam²³ as a model for the study of the approach to thermal equilibrium, although their study did not reveal an approach to equilibrium. Additional studies of this system have been made by Ford and Waters,²⁴ by Jackson,²⁵ and perhaps most interestingly by Kruskal and Zabusky.²⁶ However, Izrailev and Chirikov²⁷ were the first to suggest that Hamiltonian (9) should exhibit a KAM instability leading to statistical behavior. Zabusky and Deem²⁸ investi-

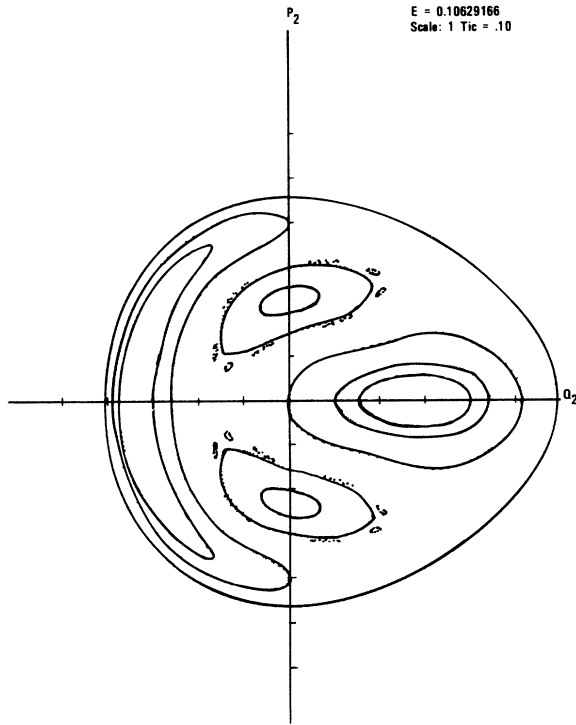


FIG. 2. Level curves for the Henon-Heiles system. The onset of macroscopic KAM instability is seen in the two chains of eight islands.

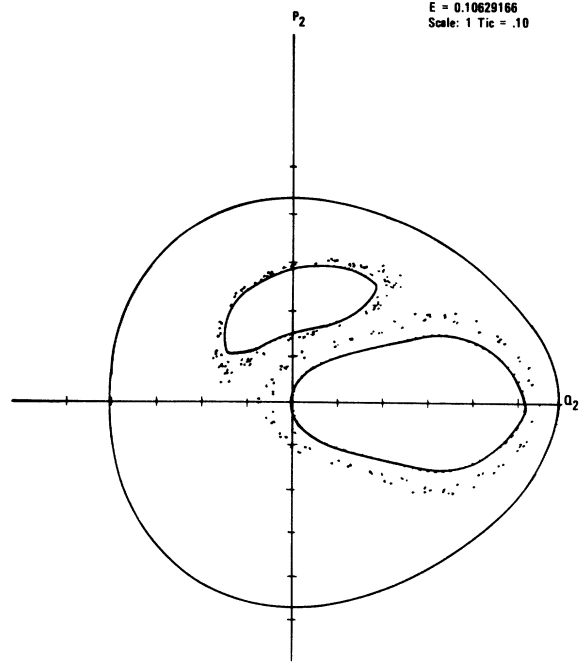


FIG. 3. Level curves for the Henon-Heiles system. This figure is a continuation of Fig. 2, using the same energy, and shows two macroscopic zones of KAM instability. The zone of instability centered on the p_2 axis encompasses the chain of eight islands shown in the upper part of Fig. 2.

gated this possibility and they demonstrated that the large amplitude motion, contrary to the small amplitude motion, does indeed exhibit widespread energy sharing among the harmonic modes. Nonetheless, complete equipartition of energy was not achieved and the motion exhibited correlations inconsistent with complete ergodicity or thermal equilibrium. At present, it is unclear whether Zabusky and Deem were observing incomplete KAM instability such as that observed in Fig. 4 or whether they were observing the constant high-order correlations of the type derived by Prigogine and co-workers.²⁹

While there can be little doubt that KAM instability is the source of the amplitude instabilities observed in the above computer experiments, the theorist's ability to predict the onset and completion of macroscopic instability is less certain. Certainly, the three recent papers^{27, 29, 30} attacking this problem have treated quite complicated systems for which prediction is especially difficult. Consequently, in this paper, we attempt to illustrate the origins and verifiably predict the onset of macroscopic amplitude instability using extremely simple oscillator models. Our intent is to provide an elementary introduction to KAM instability and to provide a reasonably accurate calculational scheme for predicting this instability

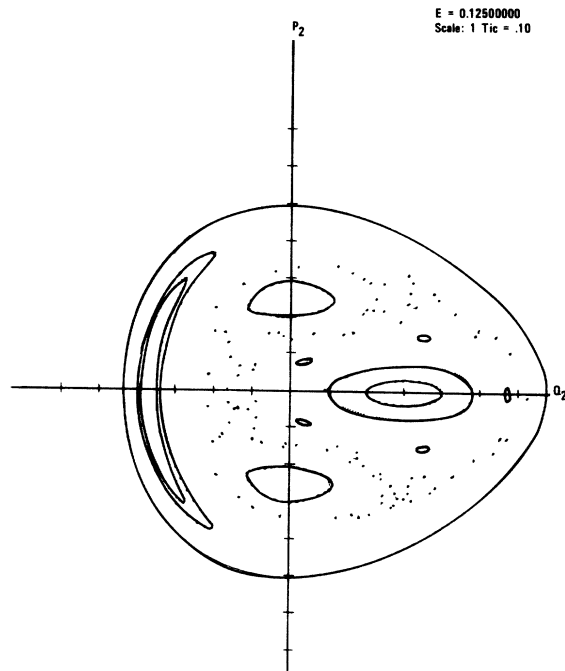


FIG. 4. Level curves for the Henon-Heiles system showing the increase in the zone of instability with increasing energy.

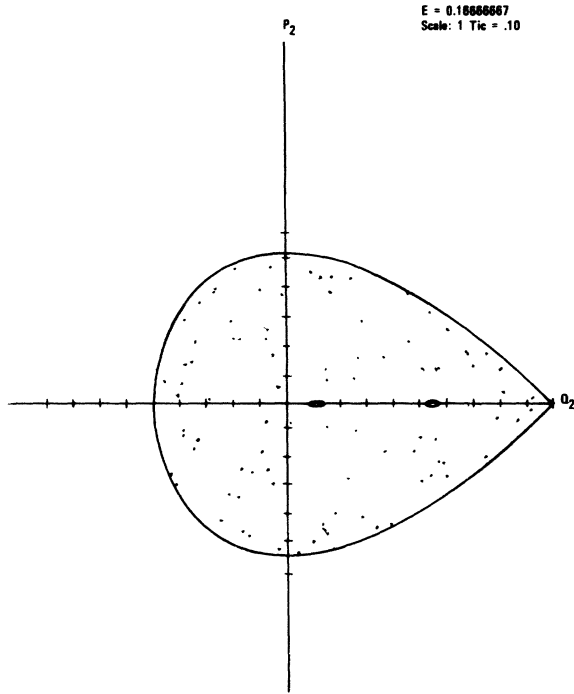


FIG. 5. Level curves for the Henon-Heiles system. The isolated dots represent the level curve for a single trajectory; however, integration accuracy for this highly unstable orbit is questionable.

alternative to those previously suggested. In Sec. II, we study the effects of isolated resonant terms on the unperturbed tori; in Sec. III, we consider the simultaneous action of two resonant terms and show that they are sufficient to demonstrate a predictable instability. Section IV relates our results to the Henon-Heiles system, and Sec. V presents our conclusions.

II. ISOLATED RESONANCES

In this section, we illustrate the distortion of unperturbed tori caused by isolated angle-dependent resonant terms. The Hamiltonians we consider are of the form

$$H = H_0(J_1, J_2) + f_{mn}(J_1, J_2) \cos(m\varphi_1 + n\varphi_2), \quad (10)$$

where $\omega_i = \partial H_0 / \partial J_i$ are both positive and where m and n are integers such that the inequality (7) can be satisfied. For brevity, an isolated perturbation of this type is called an m - n resonance, and the associated zone of highly distorted tori, loosely specified by inequality (7), is called an m - n resonance zone. Such perturbations are especially easy to analyze since they give rise to a

well-behaved constant of the motion

$$I = nJ_1 - mJ_2, \quad (11)$$

independent of H . As a consequence, we may algebraically calculate level curves for Hamiltonian (10) in any plane we choose, thus precisely determining in profile the shape and characteristics of the m - n resonance zone. In order to ease this discussion, let us turn to some specific examples.

We begin by considering the particular unperturbed Hamiltonian

$$H_0 = J_1 + J_2 - J_1^2 - 3J_1J_2 + J_2^2 \quad (12)$$

common to all our examples. The action-angle variables (J_i, φ_i) are related to the Cartesian variables (q_i, p_i) via

$$q_i = (2J_i)^{1/2} \cos \varphi_i, \quad (13a)$$

$$p_i = - (2J_i)^{1/2} \sin \varphi_i. \quad (13b)$$

In order that the unperturbed frequencies given by

$$\omega_1 = 1 - 2J_1 - 3J_2, \quad (14a)$$

$$\omega_2 = 1 - 3J_1 + 2J_2, \quad (14b)$$

be positive, we require that the energy E lie in the range $0 \leq E \leq \frac{2}{13}$ and that the values used for the J_i lie on the branch which goes to zero with E . Now Eq. (13) may be used to show that

$$J_i = \frac{1}{2} (p_i^2 + q_i^2). \quad (15)$$

Thus the unperturbed level curves in the (q_2, p_2) plane, hereafter called the J_2 plane, are concentric circles centered on the origin since J_2 is a constant. Similarly points on the level curves in the (q_1, p_1) plane or J_1 plane, defined by $q_2 = 0$, $p_2 \geq 0$ (or equivalently $\varphi_2 = \frac{1}{2} 3\pi$), also lie on concentric circles. These circular level curves in either plane are enclosed by a bounding level curve representing the intersection of the energy surface with each plane.

We now introduce a 2-2 resonance and write

$$H = H_0(J_1, J_2) + \alpha J_1 J_2 \cos(2\varphi_1 - 2\varphi_2). \quad (16)$$

Now this system has the additional constant of the motion

$$I = J_1 + J_2. \quad (17)$$

If we now use Eq. (17) to eliminate J_2 from Eq. (16) and if we set $\varphi_2 = \frac{1}{2} 3\pi$, we obtain

$$(3 + \alpha \cos 2\varphi_1)J_1^2 - (5I + I \cos 2\varphi_1)J_1 + I + I^2 - E = 0 \tag{18}$$

as the algebraic equation for level curves in the J_1 plane. A typical level-curve diagram for Eq. (18) is shown in Fig. 6. The unperturbed circular level curves are only slightly distorted except in the 2-2 resonance zone enclosed by the self-intersecting separatrix level curve. The two self-intersection points represent distinct unstable periodic solutions while the two invariant points at the center of each crescent region represent distinct stable periodic solutions. Since the central point of each crescent represents a distinct periodic orbit, the two crescents are not a chain of two islands. The central points of an island chain represent a single periodic orbit.

For all four of the above periodic orbits, we have $\dot{J}_1 = \dot{J}_2 = (\dot{\varphi}_1 - \dot{\varphi}_2) = 0$, where a dot denotes time differentiation. For the stable periodic orbits we find

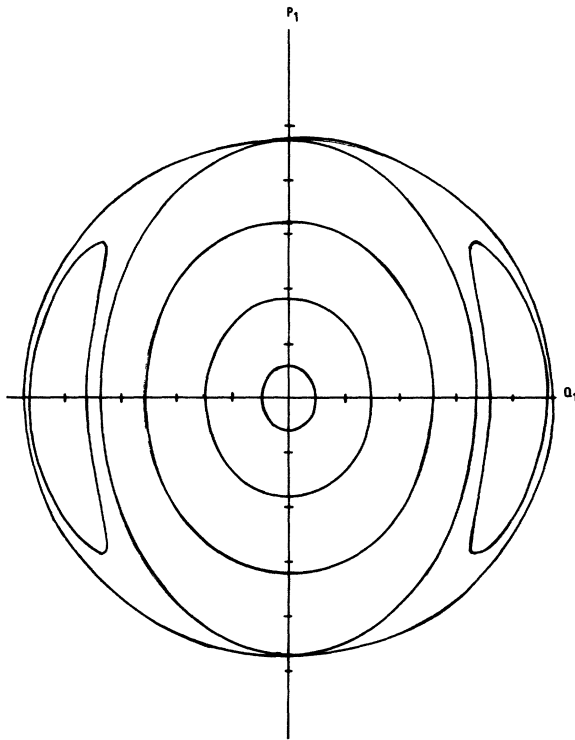


FIG. 6. Typical level curves for an isolated, 2-2 resonance computed algebraically.

$$J_1 = [(5 + \alpha)/(1 + \alpha)]J_2, \tag{19a}$$

$$(\varphi_1 - \varphi_2) = \frac{1}{2} \pi \text{ or } \frac{3}{2} \pi. \tag{19b}$$

For the unstable periodic orbits, we have

$$J_1 = [(5 - \alpha)/(1 - \alpha)]J_2, \tag{20a}$$

$$(\varphi_1 - \varphi_2) = 0 \text{ or } \pi. \tag{20b}$$

Using Eq. (14) we see that $2\omega_1 = 2\omega_2$ implies

$$J_1 = 5J_2. \tag{21}$$

Thus as predicted by the inequality (7), the 2-2 resonance zone of highly distorted tori occurs in a neighborhood of the unperturbed torus bearing the frequencies $2\omega_1 = 2\omega_2$, designated as the 2-2 torus. Putting Eq. (21) into Eq. (12), we find

$$J_1 = \frac{5}{13} [1 - (1 - \frac{13}{9} E)^{1/2}], \tag{22a}$$

$$J_2 = \frac{1}{13} [1 - (1 - \frac{13}{9} E)^{1/2}], \tag{22b}$$

as the values of J_1 and J_2 on the unperturbed 2-2 torus. Consequently, the unperturbed 2-2 torus and the perturbed 2-2 resonance zone exist for all allowed energies $0 \leq E \leq \frac{9}{13}$. As the energy increases from zero, the 2-2 resonance zone moves out from the origin and increases in width.

The closest (low-order) resonance to the 2-2 is the 3-2 or the 2-3. We investigate each. First consider

$$H = H_0(J_1, J_2) + \beta J_1^{3/2} J_2 \cos(3\varphi_1 - 2\varphi_2). \tag{23}$$

The additional constant of the motion is

$$I = 2J_1 + 3J_2, \tag{24}$$

and the level curves in the J_1 plane are given by

$$E = \frac{1}{3} I + \frac{1}{9} I^2 + (\frac{1}{3} - \frac{13}{9} I) J_1 + \frac{13}{9} J_1^2 - (\frac{1}{3} \beta) (I J_1^{3/2} - 2 J_1^{5/2}) \cos 3\varphi_1. \tag{25}$$

Typical level curves for Eq. (25) are presented in Fig. 7. Here the points at the center of each of the three crescent regions do represent a single periodic solution, and thus the 3-2 resonance zone consists of a chain of three islands. Similarly, the three self-intersecting points on the separatrix represent a single unstable periodic solution.

Again setting $\dot{J}_1 = \dot{J}_2 = (3\dot{\varphi}_1 - 2\dot{\varphi}_2) = 0$ yields

$$J_2 = (1 + 2J_1^{3/2}) / (13 + \frac{9}{12} J_1^{1/2}), \tag{26a}$$

$$(3\varphi_1 - 2\varphi_2) = \pi, 3\pi, 5\pi, \tag{26b}$$

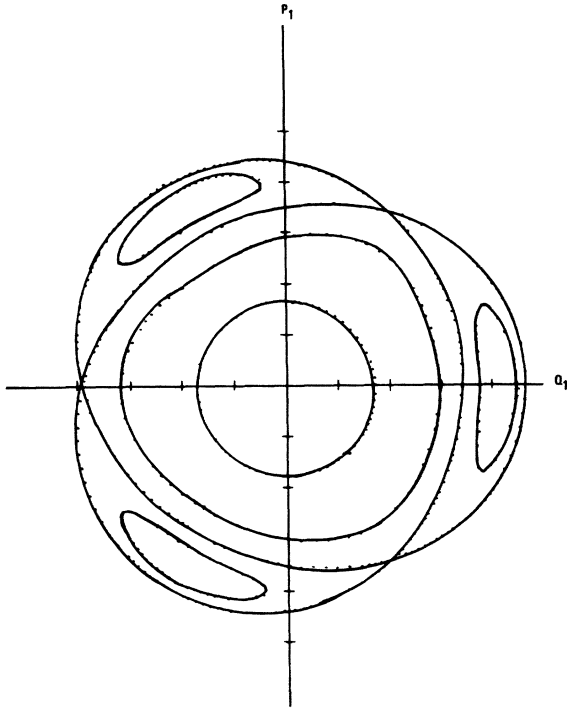


FIG. 7. Typical level curves for an isolated, 3-2 resonance computed algebraically. The dots represent points computed using Eq. (25); the curves were drawn in freehand. The chain of three islands first appears at the origin for $E = 0.08$. All the widths of the islands including this one increase with increasing energy.

for the stable periodic orbit; while

$$J_2 = (1 - 2J_1^{3/2}) / (13 + \frac{3}{2}J_1^{1/2}), \quad (27a)$$

$$(3\varphi_1 - 2\varphi_2) = 0, 2\pi, 4\pi, \quad (27b)$$

for the unstable periodic solution. As one expects, the 3-2 resonance zone lies near the unperturbed 3-2 torus. Indeed setting $3\omega_1 = 2\omega_2$ and using Eq. (12), we obtain

$$J_2 = \frac{1}{13}, \quad (28a)$$

$$J_1 = \frac{5}{13} - (\frac{3}{13} - E)^{1/2}, \quad (28b)$$

as the values of J_1 and J_2 on the unperturbed 3-2 torus where Eq. (28a) should be compared with Eqs. (26) and (27). Now Eq. (15) requires that $J_1 \geq 0$. Thus in Eq. (28b) we must have $E \geq \frac{14}{169} \approx 0.08$. At $E = \frac{14}{169}$, $J_1 = 0$. Hence the unperturbed 3-2 torus and the 3-2 resonance zone appear abruptly at the origin of the J_1 plane; they appear abruptly in the J_2 plane when the bounding level curve moves out to $J_2 = \frac{1}{13}$, i. e., at $E = \frac{14}{169}$. The fact that resonance zones in the form of island

chains may appear abruptly allows one to understand certain features of amplitude instability. For example, the onset of the instability observed by Thiele and Wilson¹⁵ is evidently due to the sudden appearance of an island chain.

Next we briefly mention the 2-3 resonance. Here

$$H = H_0(J_1, J_2) + \beta J_1 J_2^{3/2} \cos(2\varphi_1 - 3\varphi_2). \quad (29)$$

The additional constant is

$$I = 3J_1 + 2J_2. \quad (30)$$

Level curves in the J_2 plane are found from

$$E = \frac{1}{3}I - \frac{1}{9}I^2 + (\frac{1}{3} - \frac{1}{9}5I)J_2 + \frac{23}{9}J_2^2 + \beta[\frac{2}{3}J_2^{5/2} - (\frac{1}{3}I)J_2^{3/2}] \cos 3\varphi_2. \quad (31)$$

As for the 3-2 resonance, the 2-3 resonance zone appears in the J_2 plane around the unperturbed 2-3 torus which can be shown to appear abruptly at $E = 0.16$. The level curves for this resonance are quite similar to those of Fig. 7 except that the chain of three islands appears now in the J_2 plane.

These three examples suffice to give the general picture. An $m-n$ resonance for $m \neq n$ introduces a chain of m islands in the J_1 plane and a chain of n islands in the J_2 plane. Isolated resonances distort the unperturbed tori by introducing, in pairs, new stable and unstable periodic orbits. An $m-n$ resonance zone, in general, appears abruptly at some $E \geq 0$, and it is bounded by a separatrix which passes through the unstable periodic solutions. The presence of an additional simple constant of the motion allows one to calculate precisely the shape and position of each $m-n$ resonance zone. Though it is not obvious, one may show that the $m-n$ resonance zones decrease rapidly in size as m and n increase. Having now investigated isolated resonances in considerable detail, we turn to the case in which two resonances act simultaneously; we shall be especially interested in the fate of the tori in regions where the isolated resonance zones overlap.

III. DOUBLE RESONANCE

We now investigate the behavior of oscillator systems simultaneously perturbed by two isolated resonances. In particular, we wish to determine how well this behavior can be predicted. We begin by considering the Hamiltonian

$$H = H_0(J_1, J_2) + \alpha J_1 J_2 \cos(2\varphi_1 - 2\varphi_2) + \beta J_1 J_2^{3/2} \cos(2\varphi_1 - 3\varphi_2), \quad (32)$$

where $\alpha = \beta = 0.02$ in all calculations. Since the unperturbed 2-3 torus does not exist for energies $E \leq 0.16$, one may use the KAM technique indicated in Eqs. (3)–(6) to eliminate the 2-3 perturbation term. Consequently, one would expect the level curves for Hamiltonian (32) for $E \leq 0.16$ to be almost identical to those of Hamiltonian (16). This expectation is verified in Fig. 8 which presents the level curves for Hamiltonian (32), obtained by direct integration, for $E = 0.056$. Figure 8 should be compared with Fig. 6. In particular, Eq. (19a), valid for $\beta = 0$, predicts that a stable periodic orbit should occur at $q_2 = 0.142$, which to three-figure accuracy is exactly where it does occur in Fig. 8. In addition, the function $J_1 + J_2$, exactly constant for $\beta = 0$, is now constant to between four and six decimals while $3J_1 + 2J_2$ is constant only to two decimals.

Using data calculated from the equations of Sec. II, we determined that, for energies slightly greater than $E = 0.16$, the 2-2 and 2-3 resonance zones should be widely separated. Figure 9 shows the level curves for Hamiltonian (32) at $E = 0.18$. The details of Fig. 9 are accurately predicted from the data of Sec. II. Next we conjectured that a Henon-Heiles-type zone of instability might occur when the 2-2 and 2-3 resonance zones begin to

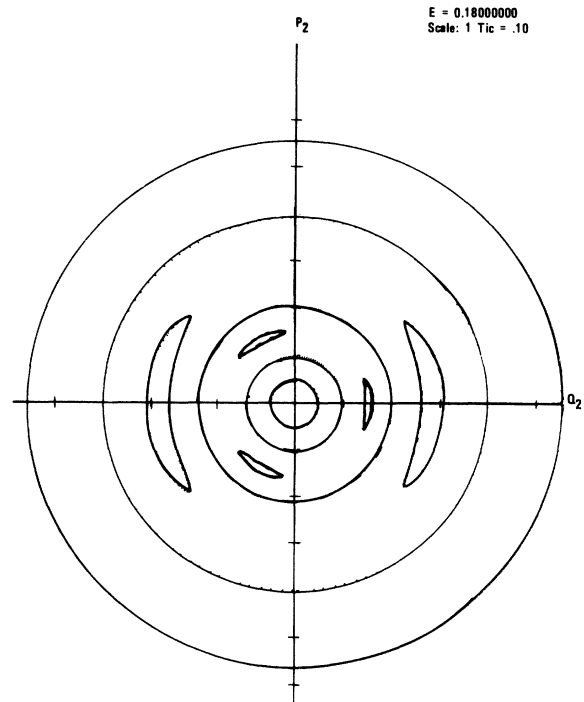


FIG. 9. Typical level curves for the 2-2, 2-3, doubly resonant Hamiltonian for energies yielding widely separated 2-2 and 2-3 resonances.

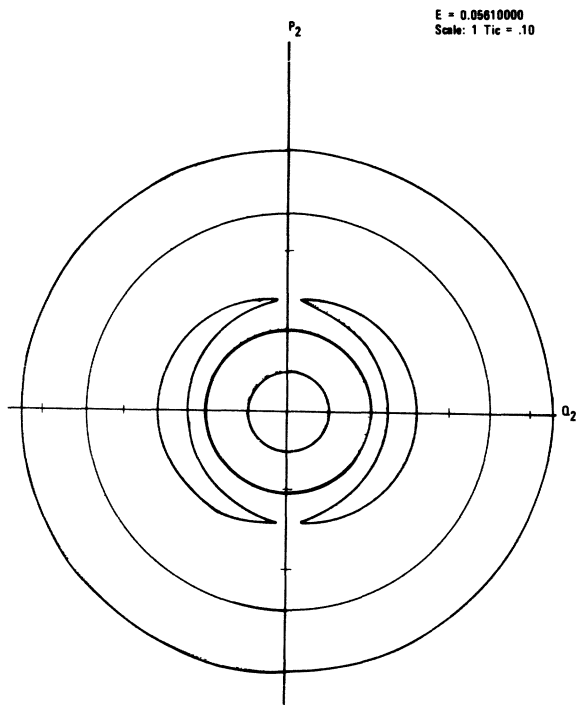


FIG. 8. Typical level curves for the 2-2, 2-3, doubly resonant Hamiltonian for energies below the appearance of the 2-3 resonance. Note the similarity to Fig. 6.

overlap. At low energies, the 2-3 zone lies inside the 2-2 zone, thus the zones should first overlap when the outer edge of the 2-3 zone touches the inner edge of the 2-2 zone. In order to estimate the energy for the onset of overlap, we calculated the q_2 -axis intercept of each zone boundary using the equations of Sec. II. In Fig. 10, we plot these q_2 intercepts as a function of energy. Overlap first occurs at energy $E = 0.2095$. In Fig. 11, we plot level curves for Hamiltonian (32), obtained by direct integration, at $E = 0.2095$. Here one observes that indeed a small zone of instability has rather abruptly appeared with the overlap of the 2-2 and 2-3 resonance zones as conjectured.

In order to illustrate the dynamics of breakdown, which is quite complicated, we show, in Fig. 12, the level curves for Hamiltonian (32) at $E = 0.20$, slightly below the predicted overlap energy. The 2-2 and 2-3 resonance zones occur in their predicted places; however, the computer also detects the chain of five islands shown in the figure but not previously predicted. There is also a detectable chain of seven islands near the chain of five which is not shown. We now discuss the origin of these higher-order resonances.

The hierarchy of resonances implicit in Hamiltonian (32) may be made explicit via the following

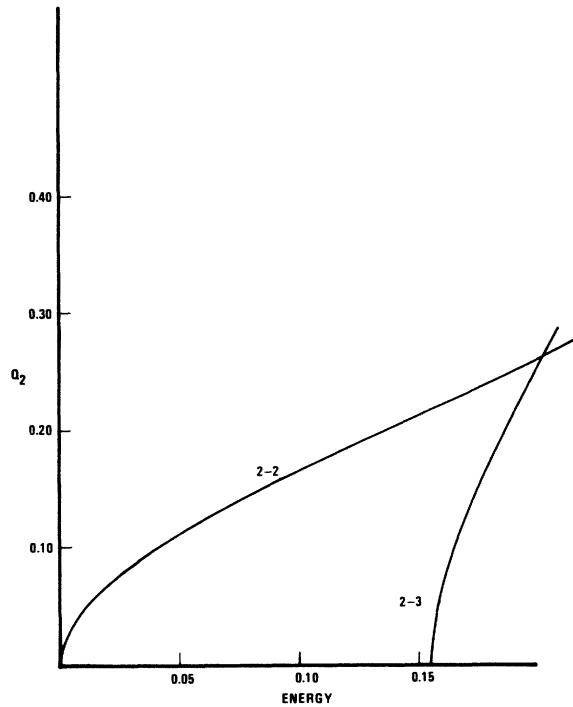


FIG. 10. q_2 -axis intercepts of the inner 2-2 and the outer 2-3 separatrices are plotted as a function of total energy.

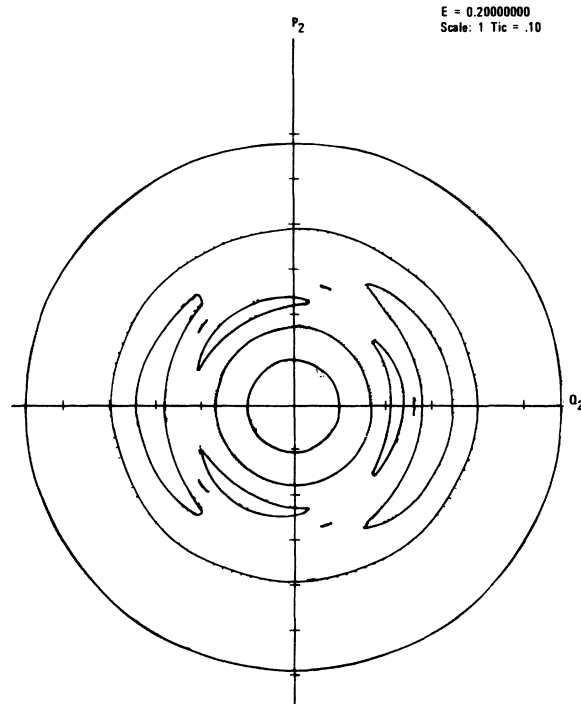


FIG. 12. Level curves for the 2-2, 2-3, doubly resonant Hamiltonian at $E=0.20$, slightly below the predicted overlap energy. The dots between the 2-2 and 2-3 crescents are part of a chain of five islands. A chain of seven islands, not shown, has also been found in this region.

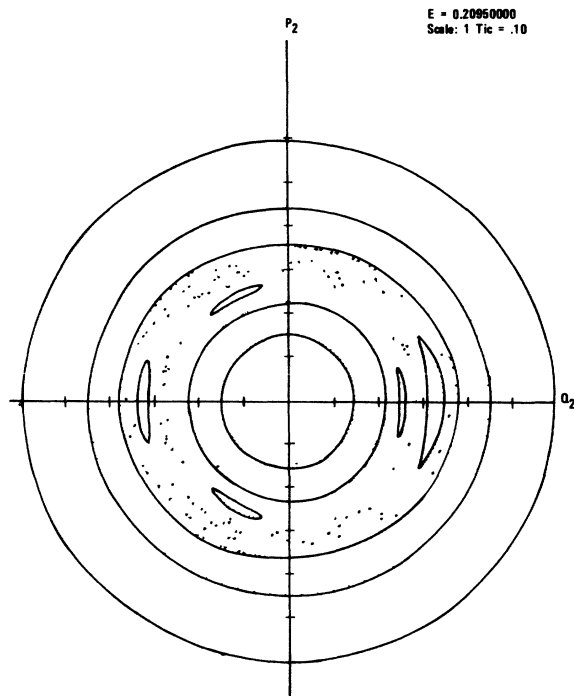


FIG. 11. Level curves for the 2-2, 2-3, doubly resonant Hamiltonian at the energy predicted for initial overlap of the 2-2 and 2-3 resonance zones.

canonical transformation formalism. Let us now regard Hamiltonian (32) as just Hamiltonian (16) perturbed by a 2-3 resonance. But Hamiltonian (16), which has a simple known constant of the motion I , is integrable²⁰; thus it is possible, though not simple,²² to determine a canonical transformation T to variables $(\mathcal{J}_i, \theta_i)$ such that the unperturbed Hamiltonian (16) is a function of the \mathcal{J}_i alone.²⁰ Denoting this new unperturbed Hamiltonian by H_1 , we have

$$H_1 = H_1(\mathcal{J}_1, \mathcal{J}_2). \tag{33}$$

In the original coordinates, typical level curves for H_1 were shown in Fig. 6; in transformed coordinates, the level curves are concentric circles centered on the origin. Under transformation T , the 2-3 resonance becomes some function $V(\mathcal{J}_1, \mathcal{J}_2, \theta_1, \theta_2)$. The full Hamiltonian (32) then becomes

$$H = H_1(\mathcal{J}_1, \mathcal{J}_2) + V(\mathcal{J}_1, \mathcal{J}_2, \theta_1, \theta_2). \tag{34}$$

If $V(\mathcal{J}_1, \mathcal{J}_2, \theta_1, \theta_2)$ is expanded in a Fourier series, then a number of new resonances will become ex-

plicit. These new resonances we shall call secondary resonances as opposed to the primary resonances explicitly appearing in Hamiltonian (32). Using the methods of Sec. II and treating each secondary resonance as if isolated, we could estimate the position and shape of each secondary-resonance-zone island chain. Transforming back to original coordinates would then reveal the position and shape of the secondary island chains. Let us note that any single resonance in Hamiltonian (34), when added to H_1 , forms an integrable system. Thus, we could repeat the process, eliminate this resonance, and reveal tertiary resonances. Indeed repeating this process to arbitrary order would reveal, upon transformation to original coordinates, a complicated network of island chains, some nested within each other.^{22, 30} The process outlined here is the germinal concept in Hamilton-Jacobi theory,²⁰ and all perturbation methods including the KAM method are various approximations which seek to reveal the nature of the Hamilton-Jacobi transformation.

It thus becomes clear that the chains of five and seven islands detected in Fig. 12 are due to secondary resonances. Rather than present the formidable calculations³¹ necessary to verify this fact, let us observe only that the chains of five and seven islands occur at precisely the positions of the unperturbed $4\omega_1 = 5\omega_2$ and $6\omega_1 = 7\omega_2$ tori calculated using Eq. (14). The following picture thus emerges. As the primary 2-2 and 2-3 resonance zones approach overlap, certain higher-order resonances begin to macroscopically distort some of the intervening preserved tori. As a consequence the narrowing region between the 2-2 and the 2-3 resonance zones contains that host of overlapping resonances, anticipated in the paragraph following the inequality (7), which yields a macroscopic zone of instability. Clearly, instability is due to a host of stable and unstable periodic orbits which now lie in a narrow region. Evidence for this instability, again at $E = 0.20$, appears in Fig. 13 where we plot a ragged level curve for an orbit near the original 2-2 separatrix. In essence then by examining the overlap of macroscopic primary resonance zones, we have illustrated on a macroscopic scale the nature of the microscopic KAM zones of instability. Moreover, we have calculated with reasonable accuracy the energy of onset for this macroscopic instability. Rather than attempting to improve this estimate by including the secondary resonances, we now seek to demonstrate that the macroscopic zone of instability grows with increasing energy.

For energies much above $E = 0.20$, the unperturbed frequencies for Hamiltonian (32) become so small that obtaining level curves by direct integration requires prohibitively long integration times. Consequently, we now increase α and β to $\alpha = 0.95$ and $\beta = 0.25$ and consider the Hamil-

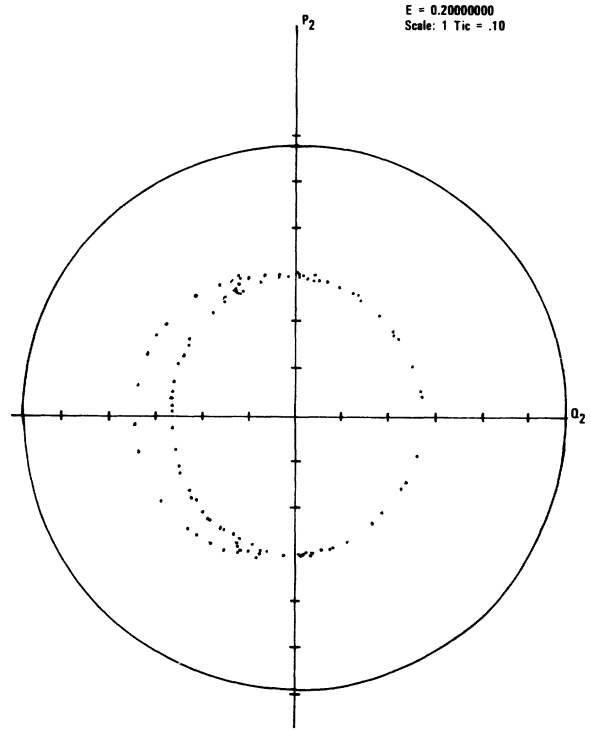


FIG. 13. This figure is a continuation of Fig. 12 and shows that a small zone of instability exists at energies below the predicted 2-2, 2-3 overlap.

tonian

$$H = H_0(J_1, J_2) + \alpha J_1 J_2 \cos(2\varphi_1 - 2\varphi_2) + \beta J_1^{3/2} J_2 \cos(3\varphi_1 - 2\varphi_2), \quad (35)$$

for which instability occurs at a lower energy. Here we choose to plot level curves in the J_1 plane, and Fig. 14 plots the q_1 intercept of the inner 2-2 and the outer 3-2 separatrix versus energy as calculated using the equations of Sec. II. Here the 3-2 resonance zone is seen to first appear at $E \cong 0.08$ while overlap is predicted at $E \cong 0.12$.

In Fig. 15, we plot level curves for energy $E = 0.05$. While these curves all appear regular, using high accuracy a chain of five islands has been detected at a radius of 0.08. The $5\omega_1 = 4\omega_2$ unperturbed torus lies at a radius of 0.098. In Fig. 16, we plot level curves for energy $E = 0.08$. The chain of five islands is now clearly visible and the 2-2 separatrix is now a small zone of instability. Instability thus occurs no later than $E = 0.08$ as compared with the predicted $E = 0.12$. Since the 3-2 resonance has not yet appeared at $E = 0.08$, it is especially clear that one cannot ignore secondary resonances here. Again, however, let us not pursue the details of secondary

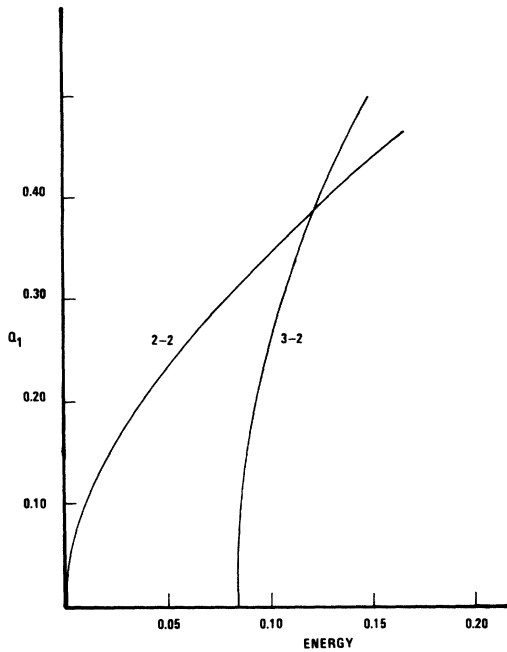


FIG. 14. q_1 -axis intercepts of the 2-2 and 3-2 separatrices are plotted as a function of total energy.

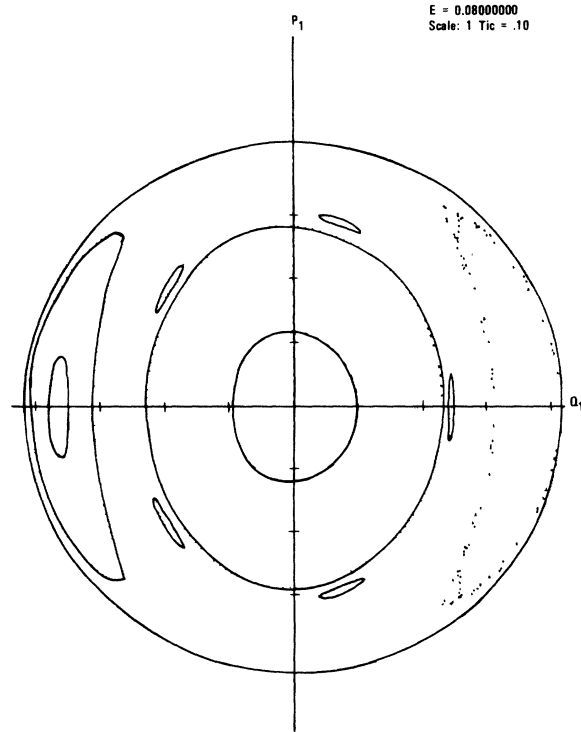


FIG. 16. Level curves for the 2-2, 3-2, doubly resonant Hamiltonian showing that a chain of islands and a zone of instability occur even before the 3-2 resonance appears.

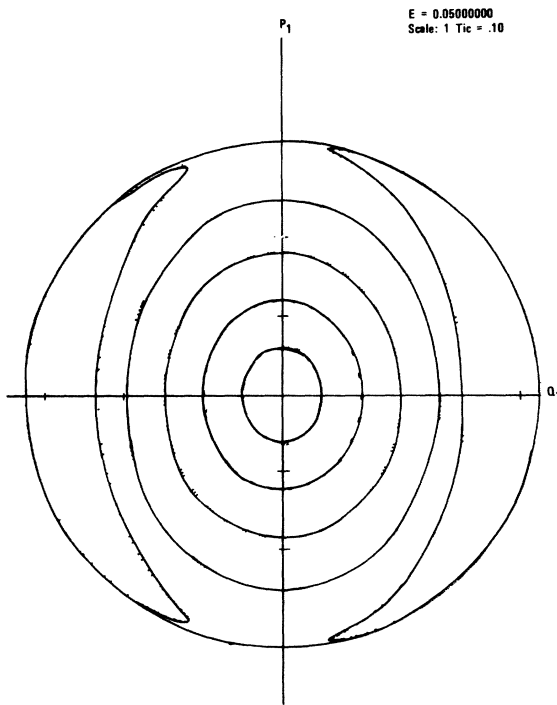


FIG. 15. Typical level curves for the 2-2, 3-2, doubly resonant Hamiltonian at low energy. Even at this low energy, a chain of five islands, not shown, has been detected.

resonance. Rather let us observe the increase in size of the zone of instability shown in Fig. 17 for which the energy has increased to $E = 0.10$. Finally, in Fig. 18 at $E = 0.14$, we see that the 3-2 resonance has at last moved into the ever enlarging zone of instability. It is now clear that our model Hamiltonians exhibit many of the characteristics of the more complicated systems previously studied. As illustration, we now turn to a discussion of the Henon-Heiles system in terms of our model Hamiltonians.

IV. RESONANCE IN TRANSFORMED COORDINATES

The isolated resonances of Sec. II were easily handled because one could without difficulty determine a well-behaved constant of the motion. Though it is less obvious, the small amplitude motion of the Henon-Heiles Hamiltonian (8) is dominated by an isolated resonance. Using a modified Birkhoff canonical transformation, Gustavson³² and independently Walker³¹ show that the Henon-Heiles Hamiltonian may be written

$$H = H_0[J_1, J_2, (\varphi_1 - \varphi_2)] + V(J_1, J_2, \varphi_1, \varphi_2) \quad (36)$$

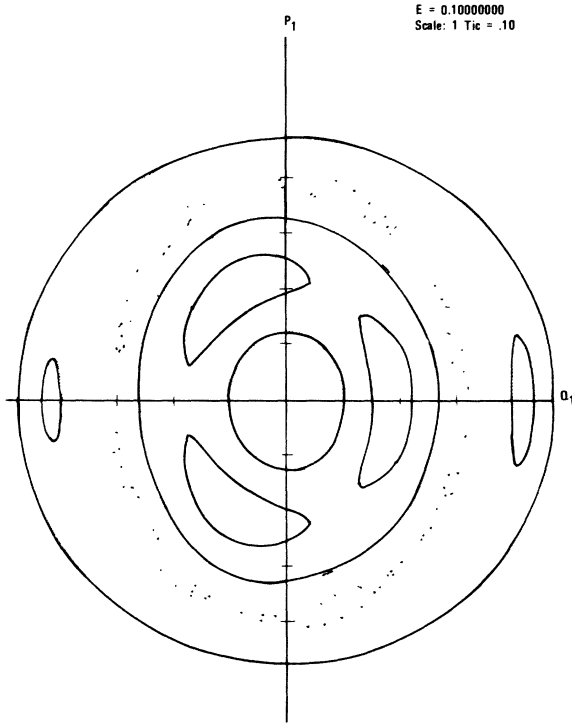


FIG. 17. Level curves for the 2-2, 3-2, doubly resonant Hamiltonian showing the increase of the instability zone with energy.

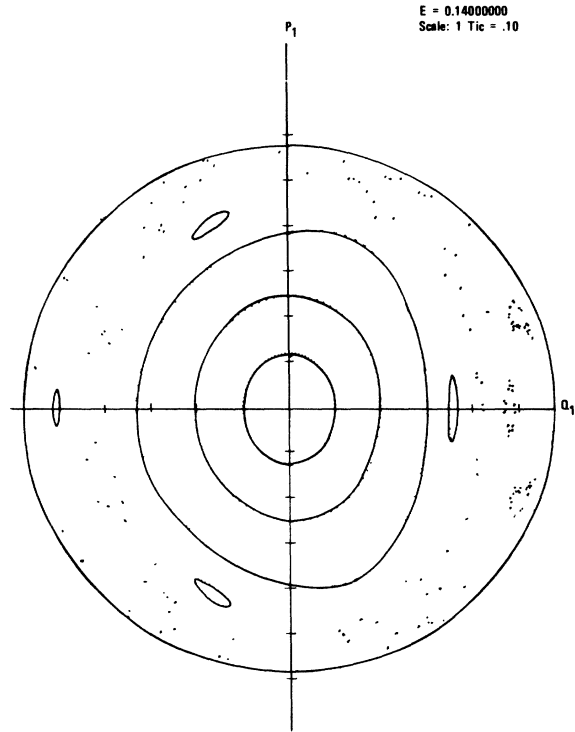


FIG. 18. Level curves for the 2-2, 3-2, doubly resonant Hamiltonian showing the 3-2 resonance as it moves into the ever-increasing zone of instability. The ragged looking chain of three islands in the right of the diagram represents a single level curve.

where V is very small compared to H_0 for sufficiently small-amplitude motion. Neglecting V , Hamiltonian (36) has the additional constant

$$I = J_1 + J_2 \quad (37)$$

One may then canonically transform Eq. (37) back to original coordinates obtaining the algebraic equation $I = I(q_1, p_1, q_2, p_2)$. This approximate constant of the motion and Hamiltonian (8) may be combined to obtain an analytic expression for level curves. For $E = \frac{1}{12}$ this expression gives level curves congruent with the directly integrated level curves of Fig. 1.

As the energy increases, the resonances in V begin to grossly distort the tori of Fig. 1. In order to determine the onset of macroscopic instability, we note that Hamiltonian (36), neglecting V , is integrable²⁰; thus there exists a canonical transformation to coordinates (j_i, θ_i) such that the full Hamiltonian (36) becomes

$$H = H_0(j_1, j_2) + V(j_1, j_2, \theta_1, \theta_2) \quad (38)$$

where H_0 is now angle-independent. Since V has a Fourier expansion, we may determine the behavior of this multiply resonant Hamiltonian in

exactly the same way as we analyzed the doubly resonant Hamiltonians of Sec. III. In essence then, the Henon-Heiles Hamiltonian is only one (compounded) canonical transformation away from the analysis of Secs. II and III. In view of the complexity of actually reducing the Henon-Heiles problem to manageable form, however, it is perhaps worthwhile illustrating by example the effects that even a simple canonical transformation can introduce.

We begin with the unperturbed Hamiltonian (12),

$$H_0 = J_1 + J_2 - J_1^2 - 3J_1J_2 + J_2^2 \quad (39)$$

For Hamiltonian (39) we recall that the level curves are concentric circles in either the J_1 or the J_2 planes. We now introduce the coordinate rotation

$$\begin{aligned} Q_1 &= (\frac{1}{2})^{1/2}(q_1 + q_2), & P_1 &= (\frac{1}{2})^{1/2}(p_1 + p_2) \quad , \\ Q_2 &= (\frac{1}{2})^{1/2}(-q_1 + q_2), & P_2 &= (\frac{1}{2})^{1/2}(-p_1 + p_2) \quad , \end{aligned} \quad (40)$$

where (q_i, p_i) are related to the (J_i, φ_i) by Eq. (13), and the (Q_i, P_i) are related to the (j_i, θ_i) via

$$Q_i = (2g_i)^{1/2} \cos\theta_i, \tag{41}$$

$$P_i = - (2g_i)^{1/2} \sin\theta_i.$$

In the variables (g_i, θ_i) , H_0 becomes

$$H_0 = g_1 + g_2 - \frac{3}{4} (g_1 + g_2)^2 + 2(g_1 + g_2)(g_1 g_2)^{1/2} \times \cos(\theta_1 - \theta_2) + 3g_1 g_2 \cos^2(\theta_1 - \theta_2). \tag{42}$$

In the g_1 (or Q_1, P_1) plane, the level curves for H_0 , originally concentric circles, become the ovals shown in Fig. 19. It is interesting to note that the level curves of Fig. 19 differ mainly from the $E = 10^{-4}$ Henon-Heiles level curves only by a 90-degree rotation (see Fig. 7 of Ref. 32). Since the Henon-Heiles Hamiltonian (36) may be written

$$H = J_1 + J_2 - \frac{5}{12} (J_1 + J_2)^2 + \frac{7}{3} J_1 J_2 \sin^2(\varphi_1 - \varphi_2) + V_2, \tag{43}$$

where V_2 is negligible for sufficiently small E , the 90-degree rotation is seen to arise because the cosine in Eq. (42) becomes a sine in Eq. (43).

Next let us consider the effect of Rotation (40) on the level curves of Hamiltonian (35), where

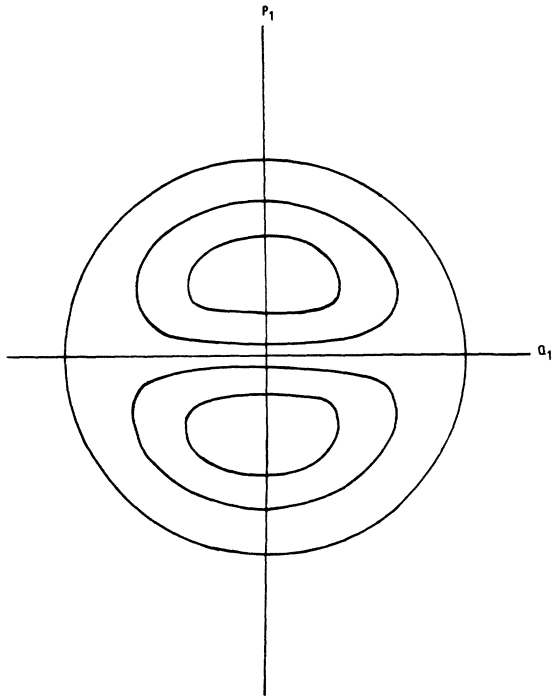


FIG. 19. Level curves for $H = J_1 + J_2 - J_1^2 - 3J_1 J_2 + J_2^2$ at $E = 0.09$ in the rotated coordinate system. If this picture is rotated by 90 degrees, one very nearly obtains the low-energy level curves for the Henon-Heiles system.

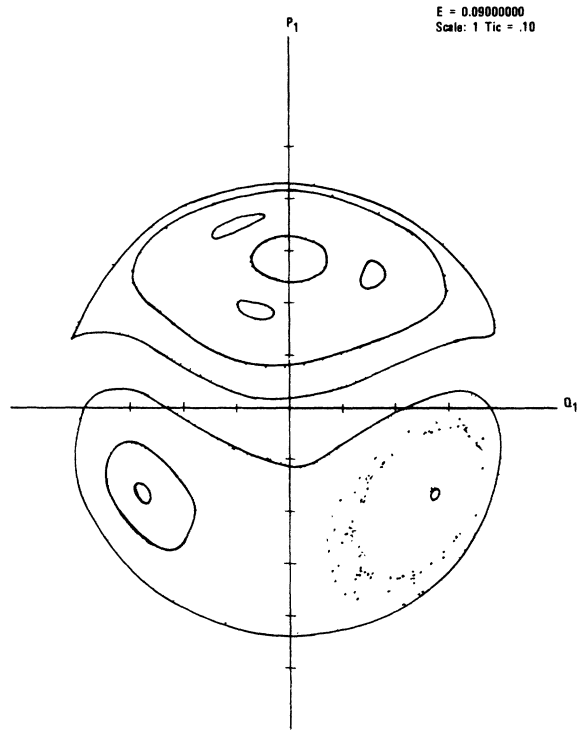


FIG. 20. Level curves for the 2-2, 3-2, doubly resonant Hamiltonian in the rotated coordinate system. These curves are close cousins of those appearing in Fig. 4.

$$H = H_0(J_1, J_2) + \alpha J_1 J_2 \cos(2\varphi_1 - 2\varphi_2) + \beta J_1^{3/2} J_2 \cos(3\varphi_1 - 2\varphi_2), \tag{44}$$

and where H_0 is given by Eq. (39). Changing variables according to Eq. (40), we may write Hamiltonian (44) as

$$H = H_0[g_1, g_2, (\theta_1 - \theta_2)] + V(g_1, g_2, \theta_1, \theta_2), \tag{45}$$

where H_0 is now given by Eq. (42) and V is a complicated but calculable function. Figure 20 shows the directly integrated, g_1 plane level curves for Hamiltonian (45) at $E = 0.09$. First, comparing Fig. 17 with Fig. 20, we see the rather dramatic distortion in level curves produced by a simple rotation of coordinates. Next, comparing Fig. 2 with Fig. 20, we see that similarity which is to be expected from the similar forms of Hamiltonians (36) and (45). In short, we have made it quite plausible that the Henon-Heiles Hamiltonian is only a coordinate transformation away from the analysis of Secs. II and III.

In concluding this section, we note that the level curves of Fig. 20 were not obtained by integrating Hamiltonian (45). Rather we integrated Eq. (44)

expressed in (q_i, p_i) coordinates and then determined the trajectory intersections with the rotated (Q_1, P_1) plane defined by $q_1 = q_2$ and $p_1 \geq p_2$. Thus geometrically speaking Figs. 17 and 20 differ only in that they represent the intersections of a given set of trajectories with two different planes. As a consequence we see that the shape of the level curves for a given Hamiltonian can dramatically depend on the intersection plane used. In particular, in order to obtain level curves for the Henon-Heiles problem similar to those of Fig. 9, instead of those shown in Fig. 1, one would have not only to rotate the intersection plane but also distort it into a curved surface. Therein lies the complexity of the Henon-Heiles problem.

V. CONCLUSIONS

For over fifty years, Poincaré's theorem on the nonexistence of well-behaved constants of the motion (other than the total energy) has stood as a pillar in the foundations of equilibrium statistical mechanics.⁵ It provides a central argument supporting the view that states of equal energy are equally likely for an isolated system. KAM theory on the other hand proves that the nonexistence of well-behaved constants of the motion is insufficient to ensure that states of equal energy are equally likely. For sufficiently small-amplitude motion, most initial conditions lead either to motion uninfluenced by any resonances, in which each action variable is a constant, or to motion influenced by isolated resonances, in which linear combinations of the action variables are constant. The existence of these constants of the motion do not violate Poincaré's theorem since the minority of trajectories moving under the influence of many resonances are densely woven between the well-behaved majority. In addition to clarifying and perhaps reducing the significance of Poincaré's theorem, however, the KAM theory points to an amplitude instability beyond which the irregular trajectories begin to dominate and the system motion perhaps becomes statistical.³³ It is thus quite possible that KAM instability can be made a cornerstone for statistical mechanics.

In this paper, we have attempted to illustrate the origin and nature of KAM instability using simple examples. For these simple systems, we have demonstrated not only that the large-amplitude motion does indeed become quite erratic but also that the onset of the instability can, in principle, be predicted. Moreover, several computer studies (in addition to ours) show that for sufficiently large amplitudes almost all trajectories are highly erratic. In this paper, we have considered systems with only two degrees of freedom; however, the procedures used can, with considerable labor, be extended to more general systems. In order for the KAM instability to be shown to be univer-

sally relevant to statistical mechanics, however, several rather serious questions must be answered.

All the computer studies thus far discussed indicate that widespread KAM instability occurs only after the amplitude of the motion becomes quite large indeed. Physical systems, on the other hand, apparently obey the laws of statistical mechanics even at cryogenic temperatures. One must therefore establish that physically realistic models exhibit KAM instability even for small-amplitude motion. One might suggest that physical potential energies are more complicated than the cubic terms of the Henon-Heiles potential or that physical systems have an enormous number of particles. However, Thiele and Wilson¹⁵ used a Morse potential in their calculations and observed instability only for energies greater than one-half the dissociation energy. Equally, Zabusky and Deem²⁸ studied Hamiltonian (9) for a 200-particle system and they observed an instability only for relatively large energies. However, the work of Northcote and Potts³⁴ suggests a possible mechanism for introducing a small-amplitude instability. They used an infinitely steep hard-core repulsion superimposed on an otherwise harmonic potential between particles and obtained ergodic-type behavior for almost all amplitudes. It is thus quite possible that an extremely steep repulsive hard-core potential could be responsible for small-amplitude instability in physical systems. Such a nonlinearity would, in addition, cause those rather sharply defined "collisions" between harmonic normal modes usually assumed in statistical mechanics. Nonetheless, whatever the conjecture, the general existence of a small-amplitude instability for physically realistic models has not been proved.

Moreover, erratic or statistical behavior of the system trajectory in the full phase space is not really required for statistical mechanics.^{29, 35, 36} Most physically measured quantities require only that projections of most trajectories be ergodic on some subspace of the full phase space. In short, statistical mechanics may follow from some type of "coarse graining." Consequently, even if KAM instability is applicable to a wide class of physical systems, there still might exist an equally wide class for which it is irrelevant.

Finally, there is an open question concerning the extent to which the zones of instability are in fact ergodic. In Fig. 4, for example, the unstable level curve shown does rather uniformly cover a certain zone of instability; however, successive intersection points for this orbit do not randomly fill the zone. Indeed, extremely accurate integration shows that they circle the stable invariant points in an orderly, though not regular, fashion. This rather low degree of order which persists even in zones of instability also appears in the work of Zabusky and Deem.²⁸ Successive points

in Fig. 5 do jump randomly, as pointed out by Henon and Heiles¹⁷; however, this randomness might disappear with improved integration accuracy.²¹ In short, the following situation may prevail. For small amplitudes only, a few low-order resonances influence the motion.²⁴ Here only simple measurable quantities would be correctly predicted by statistical mechanics. As the amplitudes increase a larger number of resonances become significant, allowing a wider variety of physical measurements (but not all) to be correctly predicted. In this picture the sudden onset of KAM instability would mark only a sudden increase in the predictive capacity of statistical mechanics rather than the issuance of an unrestricted license for its use.

Whatever the final resolution of these questions, we suggest that their study is fascinating. Answers would provide not only an increased understanding of irreversibility but perhaps also even a practical device for violating the second law of thermodynamics. In any event this paper represents at best only a very modest contribution toward their resolution, and much of the material in this paper will be quite familiar to that small group of astronomers, mathematicians, and physicists who have made similar or vastly superior contributions. Nonetheless, by couching the discussions in language familiar to physicists, it is our hope that these questions can attract the attention of a broader audience.

*Work supported in part by the National Science Foundation.

¹H. Poincaré, *Méthodes Nouvelles de la Mécanique Celeste* (Dover Publications, Inc., New York, 1957).

²G. D. Birkhoff, *Dynamical Systems* (American Mathematical Society Colloquium Publications, New York, 1927), p. 82.

³N. Kryloff and N. Bogoliuboff, *Introduction to Non-linear Mechanics* (Princeton University Press, Princeton, N. J., 1947).

⁴In this paper, we define ergodic motion as motion for which the time average of functions of the system variables is equal to the statistical mechanical phase-space average for all functions of physical interest and for most initial conditions. Since functions of physical interest are usually simple ones, this definition places less stringent requirements on the motion than do most earlier definitions.

⁵E. Fermi, *Z. Physik* **24**, 261 (1923).

⁶R. E. Peierls, *Ann. Physik* **3**, 1055 (1929).

⁷A. N. Kolmogorov, *Dokl. Akad. Nauk. SSSR* **98**, 527 (1954).

⁸V. I. Arnol'd, *Russian Math. Surveys* **18**, 9 (1963).

⁹J. Moser, *Nachr. Akad. Wiss. Göttingen, II Math. Physik Kl.* **1** (1962).

¹⁰V. I. Arnol'd, *Russian Math. Surveys* **18**, 85 (1963).

¹¹For a proof of the convergence of the formal series expansions used in Refs. 1-3, see J. Moser, *Math. Annalen* **169**, 136 (1967).

¹²H. Goldstein, *Classical Mechanics* (Addison-Wesley Press, Inc., Cambridge, Mass., 1951), p. 241.

¹³E. Merzbacher, *Quantum Mechanics* (John Wiley & Sons, Inc., New York, 1964).

¹⁴Since the resonant zones have width and are everywhere dense, even the casual reader will ask why all the unperturbed tori are not destroyed. In every neighborhood of a preserved torus with incommensurate frequencies there exist zones of destroyed tori loosely specified by the inequality (7). However, as m and n satisfying the inequality (7) increase, specifying successive regions destroyed by the perturbations $\cos(m\phi_1 + n\phi_2)$ which are

ever closer to the preserved tori, the width of these destroyed regions decreases since the f_{mn} decrease with increasing m and n . Thus, in order to demonstrate that a preserved torus exists, one need show only that the width of the destroyed regions are always smaller than the distance to the preserved torus. These notions are made quantitative in a rather simple fashion in a footnote on p. 299 of the paper by M. N. Rosenbluth, R. Z. Sagdeev, J. B. Taylor, and G. M. Zaslavski, *Nucl. Fusion* **6**, 297 (1966).

¹⁵E. Thiele and D. J. Wilson, *J. Chem. Phys.* **35**, 1256 (1961).

¹⁶D. Bunker, *J. Chem. Phys.* **37**, 393 (1962).

¹⁷M. Henon and C. Heiles, *Astron. J.* **69**, 73 (1964).

Similar results have also been reported by G. Contopoulos and L. Woltjer, *Astrophys. J.* **140**, 1106 (1964); W. H. Jefferys, *Astron. J.* **71**, 306 (1966); B. Barbanis, *ibid.* **71**, 415 (1966); G. Contopoulos and J. D. Hadjidermetriou, *ibid.* **73**, 86 (1968).

¹⁸G. Contopoulos, *Astron. J.* **68**, 1 (1963).

¹⁹In order to verify that the system trajectory should intersect the (q_2, p_2) plane in a curve when a well-behaved $I(q_1, p_1, q_2, p_2)$ exists, algebraically solve Eq. (8) for p_1 , taking the positive square root. Putting this expression for p_1 into the equation $I(q_1, p_1, q_2, p_2) = I_0$, we may invert to obtain $p_2 = p_2(q_1, E, q_2, I_0)$, where E and I_0 are the constant values of H and I . Setting $q_1 = 0$, now yields the (q_2, p_2) plane level-curve equation $p_2 = p_2(0, E, q_2, I_0)$. This last equation gives those (q_2, p_2) points on a system trajectory for which $q_1 = 0$ and $p_1 \geq 0$.

²⁰E. T. Whittaker, *Analytical Dynamics* (Cambridge University Press, London, 1965), p. 280 and Chap. 11. Also see Chap. 9 of Ref. 12.

²¹For the total integration times used, up to $t = 1500$ for the stable orbits, the energy was constant through six decimals. Moreover, at $t = 1500$, the velocities could be reversed and the motion integrated back to $t = 0$ maintaining four decimal accuracy. However, for the highly unstable orbits, the reversed integrations showed that the solutions were accurate only for $t < 200$ even though the energy continued to be constant to high

accuracy. Contopoulos (Ref. 30) obtains similar results.

²²W. H. Jefferys, *Astron. J.* 71, 306 (1966).

²³See Enrico Fermi: Collected Papers, Vol. II (University of Chicago Press, Chicago, 1965), p. 978.

²⁴J. Ford and J. Waters, *J. Math. Phys.* 4, 1293 (1963).

²⁵E. A. Jackson, *J. Math. Phys.* 4, 551, (1963); 4, 686 (1963).

²⁶See the review article by N. J. Zabusky, in Proceedings of the Symposium of Nonlinear Partial Differential Equations (Academic Press Inc., New York, 1967). Also see M. Toda, *J. Phys. Soc. Japan* 22, 431 (1967); 26 Suppl., 235 (1969).

²⁷F. M. Izrailev and B. V. Chirikov, *Dokl. Akad. Nauk SSSR* 166, 57 (1966) [English transl.: *Soviet Phys. - Doklady* 11, 30 (1966)]. This paper discusses undriven oscillator systems. For a discussion of the statistical behavior of driven oscillator systems, see V. A. Alekseev, *Math. Sbornik* 119, 545 (1968).

²⁸N. J. Zabusky and G. J. Deem, *J. Computational Phys.* 2, 126 (1967). Also see H. Hirooka and N. Saito, *J. Phys. Soc. Japan* 26, 624 (1969) and N. Saito, H. Hirooka, and N. Ooyama, *ibid.* 26 Suppl., 223 (1969).

²⁹G. M. Zaslavskii and R. Z. Sagdeev, *Zh. Eksperim.*

i Teor. Fiz. 52, 1081 (1967) [English transl.: *Soviet Phys. - JETP* 25, 718 (1967)]. This paper extends the general theory discussed in I. Prigogine, Non-Equilibrium Statistical Mechanics (Wiley-Interscience, Inc., New York, 1962).

³⁰G. Contopoulos, *Bull. Astron.* 2, 223 (1967).

³¹G. H. Walker, thesis, Georgia Institute of Technology, Atlanta, Ga., 1968 (unpublished).

³²F. G. Gustavson, *Astron. J.* 71, 670 (1966).

³³Physicists have long sought an underlying physical explanation for the purely mathematical probability arguments used to derive statistical mechanics from classical mechanics. The KAM zones of instability have an obvious random element in the positions of the unstable periodic orbits. The erratic path followed by a system trajectory may be attributed to "collisions" with these randomly positioned unstable periodic orbits.

³⁴R. A. Northcote and R. B. Potts, *J. Math. Phys.* 5, 383 (1964).

³⁵P. Mazur and E. Montroll, *J. Math. Phys.* 1, 70 (1960).

³⁶J. H. Weiner and W. F. Adler, *Phys. Rev.* 144, 511 (1966).